High-Throughput Acoustofluidic Self-Assembly of Colloidal Crystals

Meghana Akella[†] *and Jaime J. Juárez*[†,]*

[†]Iowa State University Department of Mechanical Engineering, 2529 Union Drive, Ames, Iowa, 50011, United States.

*Corresponding author, email: jjuarez@iastate.edu

Supplemental Information

Supplementary Movies

Movies 1 to 4 are sped up by 2.5 times the original frame rate. Movie 5 is sped up by 1.5 times the original frame rate.

1. Movie 1: 1ml_hr 80 V_pp.avi (4.38 MB): Optimum Crystal.avi (4.38 MB). Optimum crystal formation at 1 mL/hr and 80 V_{rms} without any defects.
2. Movie 2: 1 ml_hr 99 V_pp.avi (4.98 MB): Crystal formation at 1 mL/hr and 99 V_{rms}.
3. Movie 3: 3 ml_hr 99 V_pp.avi (4.83 MB): Crystal formation at 3 mL/hr and 99 V_{rms}.
4. Movie 4: 5 ml_hr 99V_pp.avi (4.99 MB): Crystal formation at 5 mL/hr and 99 V_{rms}.
5. Movie 5: 1 ml_hr 60 V_pp slip plane.avi (1.10 MB): Formation and reorientation of slip plane in a crystal formed at 1 mL/hr and 60V_{pp}.
6. Movie 6: Acoustically-assembled particles cured in a UV-curable resin to form bulk material.

1. Theory

1.1. Hydrodynamics of Colloidal Transport

The transport of colloidal particles entrained in a fluid flow and an acoustic field is modeled by the Langevin equation of motion[1],

$$m\frac{d\boldsymbol{u_p}}{dt} = 6\pi\mu a\left(K_p\boldsymbol{u_p} - K_f\boldsymbol{u_f}\right) + \boldsymbol{F_{ac}} + \boldsymbol{F_E} + m\cdot\boldsymbol{g} + \boldsymbol{F_B} \quad \text{(S1)}$$

where m is the particle mass, u_p is the particle velocity vector, μ is viscosity, a is the particle radius, u_f is the unperturbed fluid velocity vector, F_{ac} is the acoustic force experienced by the colloidal particles as they interact with an acoustic field, F_E is sum of all the electrostatic forces that interact with the colloidal particle, m·**g** is the gravitational body force and F_B is the stochastic force due to Brownian motion. The factors K_p and K_f represent the hindrance to colloidal particle transport and fluid flow as they approach a solid boundary.

1.2. Hydrodynamic Interactions

Fluid flow is driven through a square capillary in a single direction by a syringe pump. Neglecting acoustically generated flows, which are discussed below in the next section, the flow profile for a square capillary is[2],

$$u_{f,z}(x,y) = 4\frac{Q}{w^2}\sum_{n=1,3,5,\ldots}^{\infty}\sum_{m=1,3,5,\ldots}^{\infty}\frac{sin(n\pi x/w)sin(m\pi y/w)}{nm(n^2+m^2)} \quad \text{(S2)}$$

where Q is the fluid flow rate and w is inner width of the capillary. In this model, Q/w^2 represents the average fluid velocity (u_{avg}) in the capillary and the maximum fluid velocity is $u_{max} \approx 1.79u_{avg}$ for a square capillary. The colloidal particles sediment and are acoustically focused towards the center of the capillary microchannel. Near the wall at the channel centerline, the unperturbed fluid velocity is approximately[3],

$$u_{f,z}(y) = \frac{4u_{max}}{w}y \quad \text{(S3)}$$

for a value of y that is less than or equal to one particle radius.

The hindrance factor for a particle traveling parallel and perpendicular to a wall is given as[4],

$$K_{p,x} = K_{p,z} = \frac{12420\alpha^2(y)+12233\alpha(y)+431}{12420\alpha^2(y)+5654\alpha(y)+100} \tag{S4}$$

$$K_{p,y} = \frac{6\alpha^2(y)+9\alpha(y)+2}{6\alpha^2(y)+2\alpha(y)} \tag{S5}$$

where α = (y-a)/a. The rational functions provide convenient forms for expressing these hindrance factors to within ±0.1% of their exact values[5]. Goldman et al. present the hindrance to colloidal transport in shear flow near a wall as the ratio of particle translation velocity to unperturbed fluid velocity in the absence of particles[6],

$$\frac{u_{p,z}}{u_{f,z}} = \begin{cases} \frac{268725\alpha^2+14138\alpha+10}{268725\alpha^2+27869\alpha+37} & \frac{y}{a} > 1.003202 \\ \frac{8.38}{5.53-2.25\ln(\alpha)} & \frac{y}{a} \leq 1.003202 \end{cases} \tag{S6}$$

where the ratio is express as a rational function fit to the exact values. Based on this result, the factor K_f in the direction of flow is,

$$K_{f,z} = \frac{u_{p,z}}{u_{f,z}} K_{p,x} \tag{S7}$$

The hindrance factors presented here only represent the corrections due to the capillary wall. For simplicity, we neglect corrections for hydrodynamic interactions between particles. Investigation of these hydrodynamic interactions will be the subject of future work.

The work by Goldman et al. provides us with a way to interpret microparticle image velocimetry data near the wall of the capillary. The particle translation velocity, $u_{p,z}$, is measured using optical video microscopy and normalized by a factor of,

$$B = \frac{u_{p,z}}{\Gamma a} \tag{S8}$$

where $\Gamma = 4u_{max}/w$ is the effective shear rate in the capillary tube. The dimensionless height, y/a, is a function of B and we can use the data from Goldman et al. to estimate this functional form as,

$$\frac{y}{a} = \begin{cases} \frac{8809B^3 - 2604B^2 + 2623B + 1000}{8809B^2 - 2487B + 1784} & B > 0.45 \\ 1 + e^{(2.42 - 3.71/B)} & B \leq 0.45 \end{cases} \quad \text{(S9)}$$

Equation (S9) provides us with a way to connect the measured translation velocity with the particle's height above the capillary wall.

Brownian motion and thermal fluctuation interactions become significantly dominant at the sub-micrometer scale[7]. Brownian dynamics is given by the Langevin model for Brownian motion, considers that a particle is subject to a white noise due to thermal fluctuations. The diffusion of a particle far from a boundary is given by the Stokes-Einstein relationship,

$$D = \frac{kT}{6\pi\eta a} \quad \text{(S10)}$$

where D is the diffusivity of a single particle, k is the Boltzmann's constant, T is the absolute temperature, η is the viscosity of the medium and a is the radius of the particle. Long range hydrodynamic interactions exist in a suspension at low Reynold's number that can modify the mobility of a system. Brownian motion decreases considerably with an increase in the radius of the particles and the motion of the particles is defined by applied forces acting on the particles compared to the Brownian motion alone. Peclet number, defined as the ratio of fluid advection to particle diffusion, is used to estimate if Brownian motion can be neglected. Peclet number is given by[8],

$$Pe = \frac{6\pi u_p \mu a^2}{kT} \quad \text{(S11)}$$

For the case where Pe > 1, we can neglect the stochastic effects of Brownian motion and model the transport of colloids as deterministic.

1.3. Acoustic Forces

Acoustic waves are produced by a mechanically oscillating force on a given particle at the node (or antinode) depending on the particle-fluid material properties. The acoustic force acting on a spherical particle in an ideal fluid was formulated by King[9]. Gor'kov used the equation to derive the force on a small spherical body with the radius of the particle much larger than the wavelength of the sound wave[10]. The modified density factors for particle-medium systems with comparable densities and small spherical particles was given by Yosioka et.al.[11]. Acoustic energy is dominantly influenced by the compressibility and density of the fluid-particle system. The acoustic energy exerted on a small particle by an acoustic wave is given by[12,13],

$$U_{ac} = U_{comp} + U_{dens} \tag{S12}$$

$$U_{comp} = \frac{V_p}{4\rho_f \, c_f^2}\left[-2\left(\frac{\beta_s}{\beta_f} - 1\right) \langle P(x)^2 \rangle\right] \tag{S13}$$

$$U_{dens} = \frac{V_p}{4\rho_f \, c_f^2}\left[\frac{6(-\rho_s+\rho_f)}{(2\rho_s+\rho_f)k^2} \langle |\nabla P(x)^2| \rangle\right] \tag{S14}$$

where U_{comp} represents the energy contribution due to a change in compressibility resulting from the local acoustic pressure and U_{dens} models how the acoustic energy acts on the fluid-solid system when there is a density mismatch. While, P is the acoustic wave pressure, V_p is the volume of the particle, ρ is the density, c is the velocity of sound, β is the compressibility, λ is the wavelength and $k = 2\pi/\lambda$ is the wavenumber. The subscripts s and f represent the solid particle and fluid respectively. The angled brackets represent the time-averaged pressure where, $P(x) = P_o \cos(kx)\sin(\omega t)$, represents a model for acoustic pressure distribution our device. The pre-factor, P_o, is the pressure wave magnitude and ω is the pressure wave frequency.

Substituting these parameters in $F_{ac} = -\nabla U_{ac}$, where the primary acoustic pressure is given by,

$$F_{ac} = -\frac{\pi V_p \beta_m \Phi}{2\lambda} \nabla \langle P(x)^2 \rangle \quad \text{(S15)}$$

where Φ is the acoustic contrast factor is given by,

$$\Phi = \frac{5\rho_s - 2\rho_f}{2\rho_s + \rho_f} - \frac{\beta_s}{\beta_f} \quad \text{(S16)}$$

If the wave exerts a force on the particle towards the node, the particles are acoustically positive contrast particles (i.e., Φ is positive) and if the wave exerts a force towards the particle at the anti-node, the particles are acoustically negative particles (i.e., Φ is negative).

Acoustic energy is given by the equation

$$U = U_0 \left[2\left(1 - \frac{1}{\gamma C^2}\right) cos^2(kx) - 3\left(\frac{2(\gamma-1)}{2\gamma+1}\right) sin^2(kx)\right] \quad \text{(S17)}$$

The amplitude of energy equation is given by

$$U_0 = \frac{{P_0}^2}{8\rho_f {c_f}^2} V_p = \frac{2\pi}{3} a^3 E_{ac} \quad \text{(S18)}$$

The term, $E_{ac} = \frac{{P_0}^2}{4\rho_f {c_f}^2}$ is the energy density of the acoustic wave independent of the position of the wave, $\gamma = \frac{\rho_s}{\rho_f}$ and $C = \frac{c_s}{c_f}$. Figure 1A shows the normalized pressure distribution and Figure 1B shows the corresponding acoustic energy distribution of a sinusoidal standing acoustic wave propagating in the x-direction with a single node. The pressure and energy graphs shown in Figure 8 are normalized by the pressure amplitude and energy amplitude respectively. As described above, at zero acoustic pressure (i.e., the node), the acoustic energy is minimum, causing the particles to concentrate at the node and form an ordered crystal.

2. State Diagram

The density and compressibility values of polystyrene and water used to calculate the acoustic contrast factor of the system used in the state diagram are listed in Table S1.

As we increase the flow rate to 7 mL/hr, the microparticles assemble at the acoustic node but do not form ordered structures as shown in Figure S1.

3. Order Parameter Analysis

3.1. Computational Order Parameter Analysis

The average degree of hexagonal close-packing, $\langle C_6 \rangle$, is defined as the average number of nearest neighbors of a particle in an ensemble[14]. The number of nearest neighbors, N_i^c, for the particle, i, surrounded by nearest neighbors, j, is calculated within a coordination distance, r_c. The bond-angle between particles for a six-fold symmetry is given by[15]

$$\xi_6^i = \frac{1}{N_c^i} \sum_{j=1}^{N_c^i} e^{6\theta_{ij}\rho\sqrt{-1}} \qquad r_{ij} < r_c \tag{S19}$$

Equation (S19) is used to calculate the crystalline connectivity, χ_6^{ij}, given by

$$\chi_6^{ij} = \frac{\left| Re\left[\xi_6^i \xi_6^{j*}\right] \right|}{\left| \xi_6^i \xi_6^{j*} \right|} \tag{S20}$$

The ensemble is considered to be crystalline if $\chi_6^{ij} \geq 0.32$. So the nearest neighbors for a given particle can be calculated using[15],

$$C_6^i = \sum_{j=1}^{N_c^i} \begin{bmatrix} 1 & \chi_6^{ij} \geq 0.32 \\ 0 & \chi_6^{ij} < 0.32 \end{bmatrix} \tag{S21}$$

The average order parameter for the ensemble containing N particles, $\langle C_6 \rangle$ is given by,

$$\langle C_6 \rangle = \frac{1}{N} \sum_{j=1}^{N} C_6^i \tag{S22}$$

The above equations were used to calculate the ensemble order parameter $\langle C_6 \rangle$ for the experiments discussed below.

To calculate the experimental order parameter, $\langle C_6 \rangle$, the polydispersity factor was taken to be 20%. The values were based on the radial distribution graphs shown in Figure S2.

3.2. Theoretical Maximum Order Parameter Analysis

We also estimate the maximum average degree of hexagonal close-packing, $\langle C_6 \rangle$, for a defect-free crystal arrangement for a given crystal width, W_C, and crystal length, L_C, by assuming that the acoustic field confines the colloidal particles to rectangular area of variable aspect ratio, Ar_C. The expression for maximum $\langle C_6 \rangle$ based on ideal packing is,

$$\langle C_6 \rangle = 6 - \frac{[8 \cdot a \cdot W_c(1+Ar_c) - 6.93a^2]}{L_C W_C} \tag{S23}$$

$$Ar_C = 0.866 \frac{L_c}{W_c} \tag{S24}$$

where W_C and L_C can be estimated from optical microscopy measurements.

We estimate the maximum average degree of hexagonal close-packing, $\langle C_6 \rangle$, for a defect-free crystal arrangement for a given number of rows, N_T, and number of columns, N_L, using the following equations[16]:

$$\langle C_6 \rangle = \frac{6C_6 + 5C_5 + 4C_4 + 3C_3 + 2C_2}{N_T N_L} \tag{S25}$$

The number of particles surrounded by 6, 5, 4, 3 and 2 particles as shown in Figure S3, in a crystal confined to a rectangular area are given by,

$$C_6 = (N_T - 2)(N_L - 2) \tag{S26}$$

$$C_5 = (N_T - 2) \tag{S27}$$

$$C_4 = 2(N_L - 2) \tag{S28}$$

$$C_3 = N_T \tag{S29}$$

$$C_2 = 2 \tag{S30}$$

Substituting the Equation (S2) to (S6) in the order parameter equation, Equation (S1), we find that $\langle C_6 \rangle$ is given by

$$\langle C_6 \rangle = 6 - \frac{4N_T(1+Ar) - 2}{N} \tag{S31}$$

$$Ar = \frac{N_L}{N_T} \tag{S32}$$

where Ar is the aspect ratio of the crystal and $N = N_T \cdot N_L$ is the total number of particles in a crystal.

From Figure S3, we see that the relation between the number of columns in a crystal, N_L, and the length of the crystal, L_C, from optical microscopy is given by:

$$N_L = \frac{L_C}{2a} \tag{S33}$$

As shown in Figure S4, the distance between two rows in a crystal is given by

$$D_{row} = \sqrt{3}a \tag{S34}$$

The relation between number of rows in a crystal, N_T, and the width of the crystal obtained from optical microscopy, W_c, is given by,

$$N_T = \frac{W_c}{\sqrt{3}a} \tag{S35}$$

Substituting Equation (S9) and (S11) in Equation (S9), we get the order parameter, $\langle C_6 \rangle$, in terms of the length and width of the crystal measured using optical microscopy as

$$\langle C_6 \rangle = 6 - \frac{[8 \cdot a \cdot W_c(1+Ar_c) - 6.93a^2]}{L_C W_C} \tag{S36}$$

$$Ar_C = 0.866 \frac{L_c}{W_c} \tag{S37}$$

4. Throughput Calculation

The number of rows in a crystal for the width calculated in Figure 6 is given by Equation (S35). The number of particles entering the acoustic field (i.e., the capillary) per row, N_p, is given by,

$$N_p = \frac{Longitudinal\ Velocity}{Diameter\ of\ a\ particle} \tag{S38}$$

From Eq. (S35) and Eq. (S38), the throughput in particles per minute is given by,

$$Throughput = N_p N_T$$

$$Throughput = 17.32 \frac{W_c}{a^2} (Longitudinal\ Velocity) \quad \text{(S39)}$$

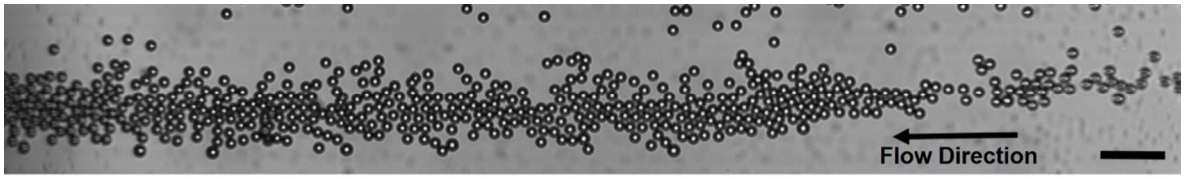

Figure S1 – A random dispersion exhibits no hexagonal ordering at 7 mL/hr and 99 V_{pp}, but the acoustic field is sufficiently strong to cause migration toward the capillary center. Scale bar is 100 μm.

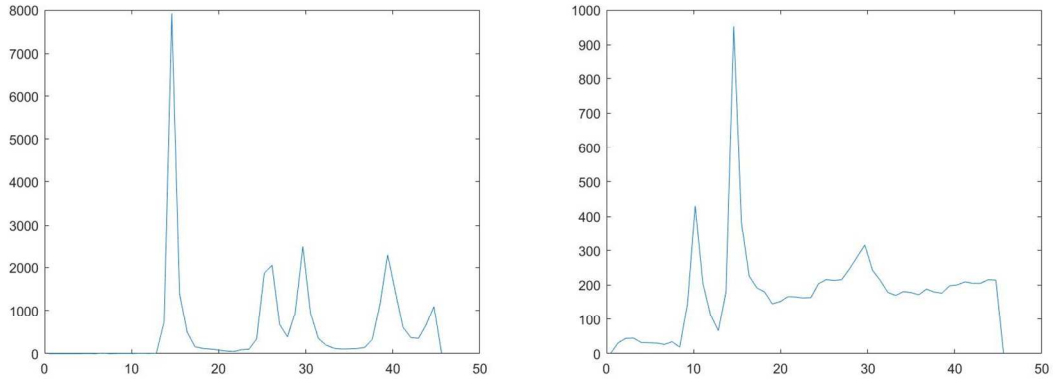

Figure S2 shows the radial distribution curves for the 1 mL/hr- 80 V_{pp} and the 5 mL/hr-60 V_{pp} cases as they are the most crystalline and least crystalline cases. A polydispersity factor of 20% for the experimental order parameter analysis was decided based on the width of the peaks.

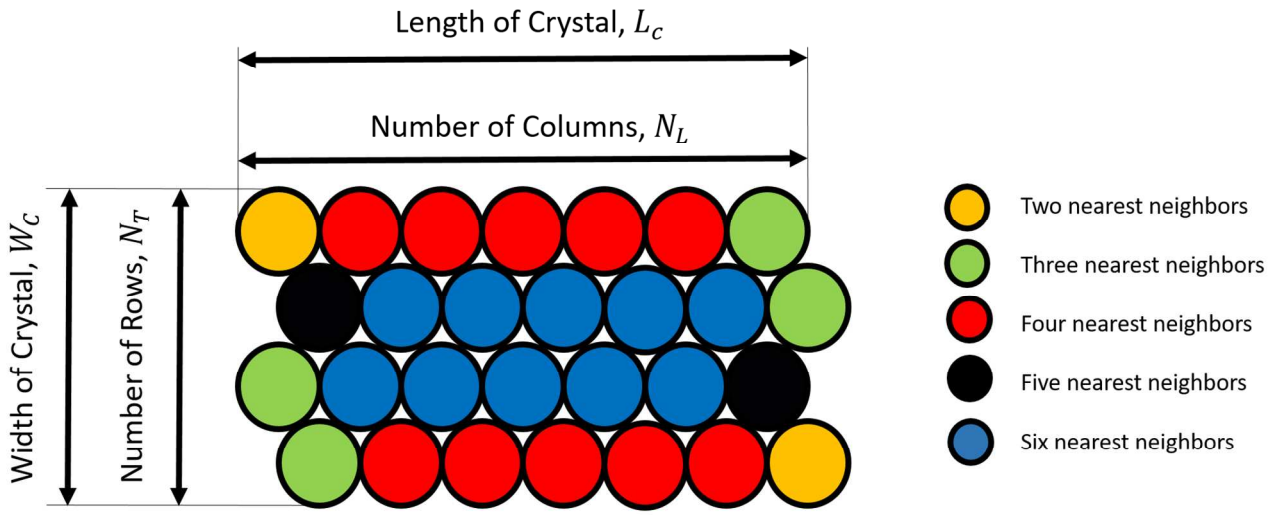

Figure S3. Schematic of the length and width convention in a crystal and the number of nearest neighbors.

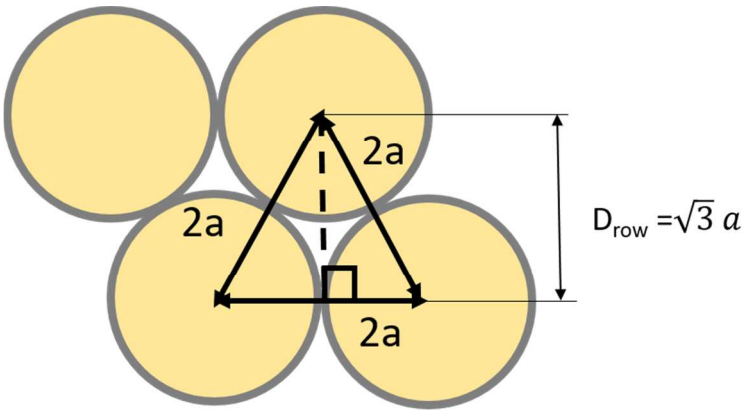

Figure S4. Schematic showing the relation between row distance, D_{row} and diameter of the particle.

Table S1. Material Properties of Water and Polystyrene[13]

	Water	Polystyrene
ρ (kg/m^3)	1000	1050
β (Pa^{-1}) / 10^{10}	3	4.58

Table S2. Theoretical Average Height of the Particle from the Capillary and Throughput

Flow Rate (mL/hr)	*Effective Shear Rate (1/s)*	*Voltage (V_{pp})*	*Experimental Average Velocity (μm/s)*	*Average Separation (nm)*	*Peclet Number (Pe)*	*Throughput Rate (Particles/min)*
1	2.0	60	6.0	7.7	1365.3	480
		80	5.4	3.2	1246.0	237.6
		99	1.1	N/A	261.6	57.18
3	6.0	60	18.8	12.3	4314.0	902.4
		80	19.4	16.2	4451.6	465.6
		99	18.6	11.2	4268.1	595.2
5	9.9	60	30.1	8.6	6906.9	1324.2
		80	34.8	29.7	7985.4	974.4
		99	34.3	26.4	7870.7	823.2

References

(1) Kim, M.; Zydney, A. L. Effect of Electrostatic, Hydrodynamic, and Brownian Forces on Particle Trajectories and Sieving in Normal Flow Filtration. *J. Colloid Interface Sci.* **1**, *269* (2), 425–431.

(2) Spiga, M.; Morino, G. L. A Symmetric Solution for Velocity Profile in Laminar Flow through Rectangular Ducts. *Int. Commun. Heat Mass Transf.* **1994**, *21* (4), 469–475.

(3) Staben, M. E.; Zinchenko, A. Z.; Davis, R. H. Motion of a Particle between Two Parallel Plane Walls in Low-Reynolds-Number Poiseuille Flow. *Phys. Fluids* **2003**, *15* (6), 1711–1733.

(4) Happel, J. B., H. *Low Reynolds Number Hydrodynamics with Special Applications to Particulate Media*, 1st ed.; Springer Netherlands, 1983.

(5) Anekal, S. G.; Bevan, M. A. Self-Diffusion in Submonolayer Colloidal Fluids near a Wall. *J. Chem. Phys.* **2006**, *125* (3), 034906.

(6) Goldman, A. J.; Cox, R. G.; Brenner, H. Slow Viscous Motion of a Sphere Parallel to a Plane wall—II Couette Flow. *Chem. Eng. Sci.* **1967**, *22* (4), 653–660.

(7) Climent, E.; Maxey, M. R.; Karniadakis, G. E. Dynamics of Self-Assembled Chaining in Magnetorheological Fluids. *Langmuir* **2004**, *20* (2), 507–513.

(8) Semwogerere, D.; Morris, J. F.; Weeks, E. R. Development of Particle Migration in Pressure-Driven Flow of a Brownian Suspension. *J. Fluid Mech.* **2007**, *581*, 437–451.

(9) King, L. V. On the Acoustic Radiation Pressure on Spheres. *Proc. R. Soc. Lond. Ser. - Math. Phys. Sci.* **1934**, *147* (861), 212.

(10) Gor'kov, L. P. On the Forces Acting on a Small Particle in an Acoustical Field in an Ideal Fluid. *Sov. Phys. Dokl.* **1962**, *6*.

(11) Yosioka, K.; Kawasima, Y. Acoustic Radiation Pressure on a Compressible Spherical. *Acta Acust. United Acust.* **1955**, *5* (3), 167–173.

(12) Barnkob, R.; Augustsson, P.; Laurell, T.; Bruus, H. Measuring the Local Pressure Amplitude in Microchannel Acoustophoresis. *Lab. Chip* **2010**, *10* (5), 563–570.

(13) Owens, C. E.; Shields, C. W.; Cruz, D. F.; Charbonneau, P.; Lopez, G. P. Highly Parallel Acoustic Assembly of Microparticles into Well-Ordered Colloidal Crystallites. *Soft Matter* **2016**, *12* (3), 717–728.

(14) Juárez, J. J.; Bevan, M. A. Feedback Controlled Colloidal Self-Assembly. *Adv. Funct. Mater.* **2012**, *22* (18), 3833–3839.

(15) Nelson, D. R.; Halperin, B. I. Dislocation-Mediated Melting in Two Dimensions. *Phys. Rev. B* **January 3**, *19* (5), 2457–2484.

(16) Juarez, J. J.; Mathai, P. P.; Liddle, J. A.; Bevan, M. A. Multiple Electrokinetic Actuators for Feedback Control of Colloidal Crystal Size. *Lab. Chip* **2012**, *12* (20), 4063–4070.